Application of refined beam elements to the coupled-field analysis of magnetostrictive microbeams

S.A. Sheikholeslami[a], M.M. Aghdam[a], E. Zappino[b,*], E. Carrera[b]

[a]*Department of Mechanical Engineering, Amirkabir University of Technology, Hafez Ave., Tehran, Iran.*
[b]*Department of Mechanical and Aerospace Engineering, Politecnico di Torino, Cso. Duca degli Abruzzi 24, 10129 Torino, Italy.*

Abstract

Bending of magnetostrictive unimorph microbeams is investigated using a one-dimensional refined finite element model based on the Carrera Unified Formulation. Since these type of smart devices are usually being used in low magnetic fields, the linear coupled magneto-mechanical constitutive relations are used to characterize their coupling behavior. With the use of the principle of virtual displacement, components of the fundamental nucleus matrix are obtained and the governing equations are discretized. 2, 3 and 4-node beam elements are used for modelling the beam major axis while linear 4-node and quadratic 9-node Lagrange elements are used as expansion functions over the cross-section. Two examples of unimorph micro-devices are considered and the results of present work are compared with those of experimental and conventional finite element works existing in the literature. It is shown that the one-dimensional refined finite element model, which is capable of generating three-dimensional results, can accurately catch the experimental data with a lower computational cost than the classical models.

Keywords: A. Smart Materials, B. Microstructures, B. Magnetic Properties, C. Finite element analysis (FEA), Carrera Unified Formulation.

1. Introduction

Magnetostrictive-based sensors and actuators are widely used in high-tech MEMS recently. In such smart devices, thin films made of special magnetostrictive materials are bonded to a non-magnetic substrate to produce bending when subjected to magnetic fields. Since special magnetostrictive materials like Terfenol-D ($Tb_xDy_{1-x}Fe_2$) are able to produce high magnetic strains [1], they can be used in such sensitive devices. Some other materials like Terbium-iron (Tb-Fe) and Samarium-Iron (Sm-Fe) alloys are also reported to produce relatively high magnetostriction in low magnetic fields [2, 3]. In the past years, some experimental and computational researches have been done to fabricate and develop magnetostrictive devices. Honda et al. [4] used a classical method to analyze the bending behavior of fabricated magnetostrictive bimorph cantilever actuators and traveling machines composed of TbFe and SmFe thin films on a polyimide substrate. Quandt et al. [5] studied the influence of the preparation conditions on the composition, microstructure, and in-plane magnetostrictive properties of amorphous thin Sm-Fe and Terfenol-D films. The authors [5] also used the finite element (FE) method to predict the maximum deflection of a silicon microbeam coated with Terfenol-D patches. A new

*Corresponding author. Tel.:+98 21 6454 3429; fax: +98 21 6641 9736.
Email address: enrico.zappino@polito.it (E. Zappino)

magnetostrictive multilayer which combine giant magnetostrictive layers and layers with large magnetic polarization was reported by Quandt et al. [6]. The high magnetostriction at low magnetic fields and the possibility of engineering material properties through the layer thickness variation were reported to be the important features of this new multilayer. Some applications of multilayered magnetostrictive devices like membrane-type micropumps, linear ultrasonic motors and optical scanners are well-discussed in the literature [7–10].

Advances in fabrication and application of multilayered magnetostrictive structures led to a variety of theoretical modellings. Some analytical models were proposed to study the static behavior of magnetostrictive bilayers. Klokholm [11] proposed a formula to relate the magnetostriction of a thin magnetostrictive film deposited on a cantilever substrate to its deflection. This formula, however, was criticized by du Tremolet de Lacheisserie and Peuzin [12]. They observed that the proposed formula of Klokholm predicts the magnetostrictive strains about twice as large as the ones actually observed. This fact led them to derive a new formula based on a more realistic energy minimization method. This method was then extended to analysis of three different systems of magnetostrictive bilayers [13]. Some other analytical works can also be found in the open literature [14–17]. Based on the finite element (FE) method, some numerical modelings of magnetostrictive unimorphs are developed. With the use of ANSYS commercial finite element code, Watts et al. [18] analyzed the magnetostriction of a bilayer cantilever through an analogous anisotropic thermal expansion simulation. Based on a weak formulation, Benbouzid et al. [19] studied the magnetomechanical coupling of magnetostrictive thin films with a two-dimensional finite element model. Body and Reyne [20] presented strong formulations and modeled magnetomechanical coupling in giant magnetostrictive thin films. Si and Cho [21] stated that the previous FE models are not applicable to a general variety of magnetostrictive actuators, including different geometries and multilayer configurations. In order to overcome these problems, they presented an FE model including beam and plate elements and applied it to the magnetomechanical coupling of magnetostrictive multilayers. In this model, six-degrees of freedom (6-DOF) beam and twelve-degrees of freedom (12-DOF) plate elements are used to model the bending of magnetostrictive multilayers. Some refined FE formulations have recently been developed to deal with elements with more DOFs. It has been shown that these higher-order elements can accurately model the deformations of complex structures with less computational cost than the conventional full three-dimensional FE models. One of these refined finite element formulations which is the basis of present work is the well-known Carrera Unified Formulation (CUF). According to the CUF, higher-order kinematics can be hierarchically developed in an automatic manner [22]. The principal characteristic of CUF models is that the order of the theory is a free parameter of the analysis. Hence, in a FEM framework, classical and arbitrarily refined elements can be formally developed by using the same formulation. This makes CUF a valuable tool to evaluate the accuracy of any structural model in a unified manner and gives the capability of generating three-dimensional results with one-dimensional formulations [23–25]. CUF has been successfully applied to thin-walled structures [26, 27], buckling problems [28], free vibration and dynamic response analyses [29, 30], composite structures [31, 32] and component-wise analysis of aerospace and civil structures [23, 33]. This formulation has also been successfully applied to coupled multifield analyses, like thermo-mechanical [34–36], electro-mechanical [37, 38], and mixed thermo-electro-mechanical [39, 40] problems. The main aim of the present work is to apply the one-dimensional CUF to magneto-mechanical coupling analysis of magnetostrictive micro-devices.

2. One-dimensional refined FE model based on Carrera Unified Formulation

There are 4 generalized displacement parameters when dealing with magnetomechanical coupling analysis of structures. These parameters are

$$\mathbf{u} = \left\{ \begin{array}{cccc} u_1 & u_2 & u_3 & \varphi \end{array} \right\}^T \tag{1}$$

where u_1, u_2 and u_3 are components of the displacement field and φ denotes the magnetic potential. The generalized strain and stress vectors can be defined as

$$\mathbf{X} = \left\{ \begin{array}{ccccccccc} \varepsilon_{11} & \varepsilon_{22} & \varepsilon_{33} & \varepsilon_{23} & \varepsilon_{13} & \varepsilon_{12} & H_1 & H_2 & H_3 \end{array} \right\}^T \tag{2}$$

$$\mathbf{Y} = \left\{ \begin{array}{ccccccccc} \sigma_{11} & \sigma_{22} & \sigma_{33} & \sigma_{23} & \sigma_{13} & \sigma_{12} & B_1 & B_2 & B_3 \end{array} \right\}^T \tag{3}$$

where σ, ε, B and H stand for stress, strain, magnetic flux density and magnetic field intensity, respectively. It should be noted that the magnetic field intensity is related to the magnetic potential as

$$\mathbf{H} = \nabla\varphi \tag{4}$$

where ∇ is the gradient operator. The generalized strain components are related to the generalized displacement components of Eq. 1 through the following relation

$$\mathbf{X} = \mathbf{D}\mathbf{u} \tag{5}$$

where the 9×4 matrix $\mathbf{D}$ is

$$\mathbf{D} = \begin{bmatrix} \frac{\partial}{\partial x} & 0 & 0 & 0 \\ 0 & \frac{\partial}{\partial y} & 0 & 0 \\ 0 & 0 & \frac{\partial}{\partial z} & 0 \\ 0 & \frac{\partial}{\partial z} & \frac{\partial}{\partial y} & 0 \\ \frac{\partial}{\partial z} & 0 & \frac{\partial}{\partial x} & 0 \\ \frac{\partial}{\partial y} & \frac{\partial}{\partial x} & 0 & 0 \\ 0 & 0 & 0 & -\frac{\partial}{\partial x} \\ 0 & 0 & 0 & -\frac{\partial}{\partial y} \\ 0 & 0 & 0 & -\frac{\partial}{\partial z} \end{bmatrix} \tag{6}$$

The linear coupled constitutive relations for piezomagnetic materials can be written in index notation as

$$\sigma_{ij} = C_{ijkl}\varepsilon_{kl} - e_{kij}H_k \tag{7}$$

$$B_i = e_{ikl}\varepsilon_{kl} + \chi_{ik}H_k \tag{8}$$

where e_{kij} and χ_{ik} are the magnetostrictive coupling constants and magnetic permeability, respectively, and the repeated indices i,j and k count for summation. With the definition of generalized stress and strain vectors (Eqs. 2 and 3), the constitutive relations can be

written in compact form as

$$\mathbf{Y} = \mathbf{R}\mathbf{X} \tag{9}$$

where the 9×9 matrix $\mathbf{R}$ is

$$\mathbf{R} = \begin{bmatrix} \mathbf{R}_{11} & \mathbf{R}_{12} \\ \mathbf{R}_{21} & \mathbf{R}_{22} \end{bmatrix} \tag{10}$$

with the submatrices defined as

$$\mathbf{R}_{11} = \begin{bmatrix} C_{11} & C_{12} & C_{13} & 0 & 0 & 0 \\ C_{12} & C_{22} & C_{23} & 0 & 0 & 0 \\ C_{13} & C_{23} & C_{33} & 0 & 0 & 0 \\ 0 & 0 & 0 & C_{44} & 0 & 0 \\ 0 & 0 & 0 & 0 & C_{55} & 0 \\ 0 & 0 & 0 & 0 & 0 & C_{66} \end{bmatrix} \tag{11}$$

$$\mathbf{R}_{21} = \mathbf{R}_{12}^T = \begin{bmatrix} 0 & 0 & 0 & 0 & e_{15} & 0 \\ 0 & 0 & 0 & 0 & 0 & e_{15} \\ e_{13} & e_{13} & e_{33} & 0 & 0 & 0 \end{bmatrix} \tag{12}$$

$$\mathbf{R}_{22} = \begin{bmatrix} \chi_{11} & 0 & 0 \\ 0 & \chi_{11} & 0 \\ 0 & 0 & \chi_{33} \end{bmatrix} \tag{13}$$

for homogeneous and orthotropic piezomagnetic materials. The principle of virtual displacement in the absence of inertial works indicates that [22]:

$$\delta L_{int} = \int_V \delta \mathbf{X}^T \mathbf{Y} dV = \delta L_{ext} \tag{14}$$

where L_{int} and L_{ext} stand for internal and external works, respectively, and δ is the variational operator. The internal work can be expressed in terms of generalized displacement vector as

$$\int_V \delta \mathbf{X}^T \mathbf{R} \mathbf{X} dV = \int_V \delta \mathbf{X}^T \mathbf{R} \mathbf{X} dV = \int_V \delta (\mathbf{D}\mathbf{u})^T \mathbf{R} \left(\mathbf{D}\mathbf{u}\right) dV \tag{15}$$

For a beam with a y-axis coinciding longitudinal axis, the 1D refined finite element model can be used to discretize the domain. In this way, the generalized displacement vector can be written as

$$\mathbf{u}(x, y, z) = N_i(y) F_\tau(x, z) \mathbf{U}_{\tau i} \tag{16}$$

where N_i denotes the 1D shape function along the beam longitudinal axis, F_τ is the Lagrange expansion function of displacement components on cross-sectional area of the beam and $\mathbf{U}_{\tau i}$ is the vector of nodal displacement components [22, 41]. The same form can also be used for describing the variation of generalized displacement vector:

$$\delta \mathbf{u}(x,y,z) = N_j(y) F_s(x,z) \delta \mathbf{U}_{sj} \tag{17}$$

Substitution of Eqs. 16 and 17 in Eq. 15 yields

$$\begin{aligned}
\delta L_{int} &= \int_V \delta(\mathbf{D}\mathbf{u})^T \mathbf{R} \left(\mathbf{D}\mathbf{u}\right) dV \\
&= \int_V \delta(\mathbf{D}N_j(y)F_s(x,z)\mathbf{U}_{sj})^T \mathbf{R} \left(\mathbf{D}N_i(y)F_\tau(x,z)\mathbf{U}_{\tau i}\right) dV \\
&= \int_V \delta \mathbf{U}_{sj}^T (\mathbf{D}N_j(y)F_s(x,z))^T \mathbf{R} \left(\mathbf{D}N_i(y)F_\tau(x,z)\right) \mathbf{U}_{\tau i} dV \\
&= \delta \mathbf{U}_{sj}^T \left(\int_V (\mathbf{D}N_j(y)F_s(x,z))^T \mathbf{R} \left(\mathbf{D}N_i(y)F_\tau(x,z)\right) dV \right) \mathbf{U}_{\tau i} \\
&= \delta \mathbf{U}_{sj}^T \mathbf{k}^{\tau sij} \mathbf{U}_{\tau i}
\end{aligned} \tag{18}$$

where the 4×4 matrix $\mathbf{k}^{\tau sij}$ is the fundamental nucleus of 1D piezomagnetic beam element. The components of this matrix are

$$
\begin{aligned}
k_{11}^{\tau sij} &= C_{11}\int_l N_i N_j dy \int_A F_{\tau,x}F_{s,x}dxdz + C_{55}\int_l N_i N_j dy \int_A F_{\tau,z}F_{s,z}dxdz \\
&\quad + C_{66}\int_l N_{i,y}N_{j,y}dy \int_A F_\tau F_s dxdz \\
k_{12}^{\tau sij} &= C_{12}\int_l N_{i,y}N_j dy \int_A F_\tau F_{s,x}dxdz + C_{66}\int_l N_i N_{j,y}dy \int_A F_{\tau,x}F_s dxdz \\
k_{13}^{\tau sij} &= C_{13}\int_l N_i N_j dy \int_A F_{\tau,z}F_{s,x}dxdz + C_{55}\int_l N_i N_j dy \int_A F_{\tau,x}F_{s,z}dxdz \\
k_{14}^{\tau sij} &= -e_{13}\int_l N_i N_j dy \int_A F_{\tau,z}F_{s,x}dxdz - e_{15}\int_l N_i N_j dy \int_A F_{\tau,x}F_{s,z}dxdz \\
k_{21}^{\tau sij} &= C_{12}\int_l N_i N_{j,y} dy \int_A F_{\tau,x}F_s dxdz + C_{66}\int_l N_{i,y}N_j dy \int_A F_\tau F_{s,x}dxdz \\
k_{22}^{\tau sij} &= C_{22}\int_l N_{i,y}N_{j,y}dy \int_A F_\tau F_s dxdz + C_{44}\int_l N_i N_j dy \int_A F_{\tau,z}F_{s,z}dxdz \\
&\quad + C_{66}\int_l N_i N_j dy \int_A F_{\tau,x}F_{s,x}dxdz \\
k_{23}^{\tau sij} &= C_{23}\int_l N_i N_{j,y} dy \int_A F_{\tau,z}F_s dxdz + C_{44}\int_l N_{i,y}N_j dy \int_A F_\tau F_{s,z}dxdz \\
k_{24}^{\tau sij} &= -e_{13}\int_l N_i N_{j,y} dy \int_A F_{\tau,z}F_s dxdz - e_{15}\int_l N_{i,y}N_j dy \int_A F_\tau F_{s,z}dxdz \\
k_{31}^{\tau sij} &= C_{13}\int_l N_i N_j dy \int_A F_{\tau,x}F_{s,z}dxdz + C_{55}\int_l N_i N_j dy \int_A F_{\tau,z}F_{s,x}dxdz \\
k_{32}^{\tau sij} &= C_{23}\int_l N_{i,y}N_j dy \int_A F_\tau F_{s,z}dxdz + C_{44}\int_l N_i N_{j,y}dy \int_A F_{\tau,z}F_s dxdz \\
k_{33}^{\tau sij} &= C_{33}\int_l N_i N_j dy \int_A F_{\tau,z}F_{s,z}dxdz + C_{44}\int_l N_{i,y}N_{j,y}dy \int_A F_\tau F_s dxdz \\
&\quad + C_{55}\int_l N_i N_j dy \int_A F_{\tau,x}F_{s,x}dxdz \\
k_{34}^{\tau sij} &= k_{43}^{\tau sij} = -e_{15}\int_l N_i N_j dy \int_A F_{\tau,x}F_{s,x}dxdz \\
&\quad - e_{15}\int_l N_{i,y}N_{j,y}dy \int_A F_\tau F_s dxdz - e_{33}\int_l N_i N_j dy \int_A F_{\tau,z}F_{s,z}dxdz \\
k_{41}^{\tau sij} &= -e_{13}\int_l N_i N_j dy \int_A F_{\tau,x}F_{s,z}dxdz - e_{15}\int_l N_i N_j dy \int_A F_{\tau,z}F_{s,x}dxdz \\
k_{42}^{\tau sij} &= -e_{13}\int_l N_{i,y}N_j dy \int_A F_\tau F_{s,z}dxdz - e_{15}\int_l N_i N_{j,y}dy \int_A F_{\tau,z}F_s dxdz \\
k_{44}^{\tau sij} &= \chi_{11}\int_l N_i N_j dy \int_A F_{\tau,x}F_{s,x}dxdz + \chi_{11}\int_l N_{i,y}N_{j,y}dy \int_A F_\tau F_s dxdz \\
&\quad + \chi_{33}\int_l N_i N_j dy \int_A F_{\tau,z}F_{s,z}dxdz
\end{aligned}
\tag{19}
$$

On the other hand, the variation of external work can be written as

$$
\delta L_{ext} = \delta \mathbf{U}_{sj}^T \mathbf{Q}_{sj} \tag{20}
$$

In this equation, $\mathbf{Q}_{sj}$ is the vector of concentrated nodal forces

$$\mathbf{Q}_{sj}^{T} = \left\{ \begin{array}{cccc} Q_1 & Q_2 & Q_3 & 0 \end{array} \right\}_{sj} \tag{21}$$

where Q_i $(i = 1, 2, 3)$ are components of external load vector in each node. Equating Eqs. 18 and 20, and assembling the fundamental nuclei matrices as well as element load vectors in a proper way leads to the following linear set of equations:

$$[\mathbf{K}]\{\mathbf{U}\} = \{\mathbf{Q}\} \tag{22}$$

Solving Eqs. 22 together with magnetomechanical boundary conditions yields the nodal values of generalized displacements.

3. Results and Discussion

As the first example, a cantilever unimorph microbeam consisting of a silicon substrate and a magnetostrictive Terfenol-D coating is considered, as shown in Figure 1. The beam is subjected to a magnetic field in the longitudinal direction. The dimensional parameters are a=5mm and b=20mm, and the tickness of Si and Terfenol-D layers are 50 μm and 10 μm, respectively. The material properties of each component are tabulated in Table 1. It should be noted that the values for magnetostrictive coupling constants are converted since ref. [42] has used *d-based* constitutive relations.

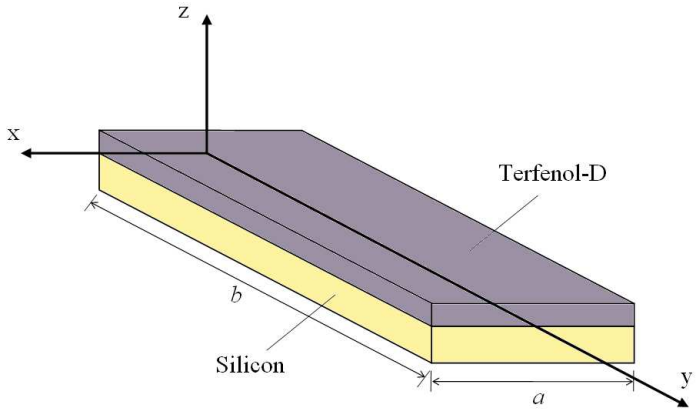

Figure 1: Cantilever magnetostrictive unimorph microbeam

In order to validate the results of present study, the tip deflection of the bilayer microbeam is compared with the results of an experimental work [5] in Table 2. In this table, 2 and 3-node beam elements (B2 and B3) are used for beam discretization while 4 and 9-node Lagrange elements (L4 and L9) are used as the expansion functions to model the cross-section, as shown in Figure 2. As it can be seen, in the region of low magnetic field intensities ($<$ 120 Oe), the present results match well the experimental data, while in moderate and high field intensities, due to the nonlinear nature of Terfenol-D, the error grows gradually.

In order to show the stress distributions, five 4-node beam elements (B4) are used in conjuction with L4 and L9 cross-sectional Lagrange elements. The micro-beam is subjected to a longitudinal magnetic field intensity of 100 Oe. The variation of normal

Table 1: Material properties of unimorph beam [5, 42]

Silicon		
Elastic modulus	169	GPa
Poissons ratio	0.067	-
Terfenol-D		
Elastic modulus	50	GPa
Poissons ratio	0	-
e_{33}	0.5	kN/Am
e_{15}	1.4	kN/Am
χ_{33}	6.29	μH/m

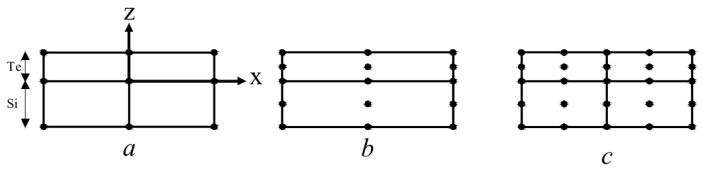

Figure 2: Cross-sectional Lagrange element configurations, *a*)4L4, *b*)2L9 and *c*)4L9

Table 2: Convergence analysis and comparison of microbeam deflection with experimental data [5]

H_2 (Oe)	u_3 (μm)				
	5B2, 4L9	5B3, 4L4	5B3, 2L9	5B3, 4L9	Ref. [5]
26.00	27.18	26.38	27.30	27.25	24.59
56.40	59.66	57.91	59.93	59.81	65.57
86.80	91.48	88.79	91.89	91.72	94.26
117.00	123.30	119.67	123.85	123.62	117.10
148.00	156.45	151.85	157.14	156.85	135.83
178.00	187.61	182.09	188.44	188.10	155.73
213.00	224.73	218.12	225.72	225.31	168.03
243.00	256.55	248.97	257.69	257.21	176.81

stress component (σ_{yy}) through the thickness direction is shown in Figure 3 for three configurations of Lagrange elements. It can be seen that L4 elements can give relatively good results compared to L9 elements. Moreover, it is clear that the neutral axis of the beam does not coincide with the substrate mid-axis when the unimorph is subjected to a magnetic field.

Since the present method can give the three-dimensional stress distribution, it is valuable to show the stress distributions in the width direction (i.e., the x-direction). Again, the cantilever beam is subjected to a-100 Oe-magnetic field. Twelve L9 elements are used in this analysis and four important shear and normal stress components are plotted versus the width of the beam in Figure 4. As it is expected, the results for normal stresses and transverse shear stress show symmetry about vertical cross-sectional axis (z-axis); However, the in-plane shear stress component (σ_{xy}) should be symmetric about the origin. Since the considered location is relatively near the clamped end of the beam, some variation in shear and normal stress components is observed. On the other hand, the transverse normal stress component (σ_{xx}) is expected to vanish at boundaries ($x = \pm 2.5$ mm), since there is no traction on these sides; But it can be seen that the model is not able to satisfy the boundary conditions at all points. More refined kinematics should in fact be used in order to achieve this result.

As a second example, a silicon substrate coated with two symmetrically located

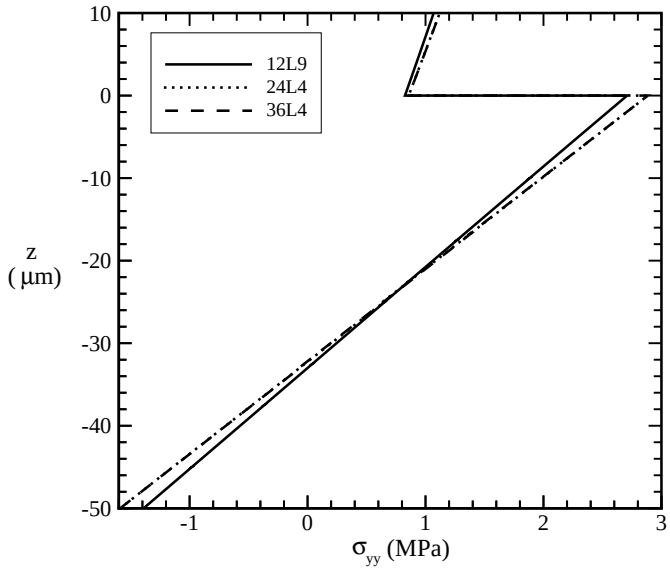

Figure 3: Distribution of normal stress σ_{yy} through the beam thickness at $x = 0$ and $y = 4$mm, for $H_2 = 100$Oe

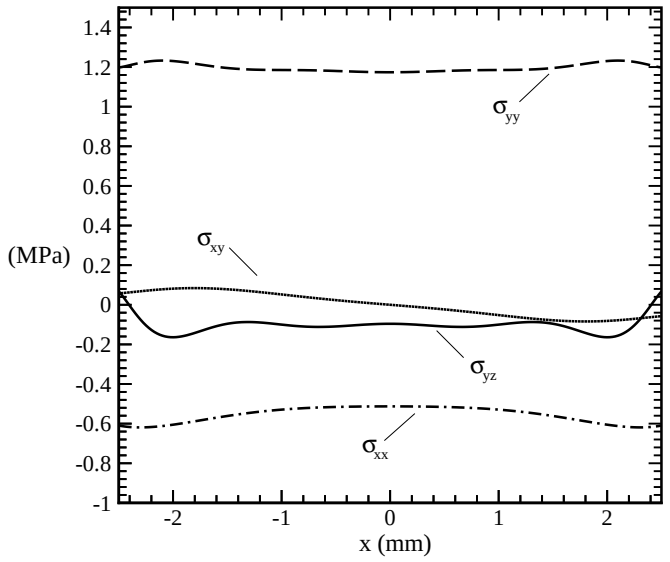

Figure 4: Distribution of shear and normal stress components in the width direction at $y = 4$mm and $z = 10\mu$m, for $H_2 = 100$Oe

Terfenol-D patches is considered (Figure 5). The dimensional parameters are a=2mm and b=10mm, and the tickness of silicon substrate and Terfenol-D patches are 50 μm and 10 μm, respectively. The microbeam is clamped at both ends and is subjected to a magnetic field in the longitudinal direction. The material properties are the same as the previous example, as shown in Table 1. In order to validate the results for this case, maximum deflection of the beam is plotted versus the length l of uncoated silicon in Figure 6. The results are compared with experimental data of [5] as well as the results from conventional FE method of [21]. In this comparison, 10B2 elements are used for

beam discretization and 4L9 elements are used to expand the displacement field in the cross-section. It can be seen that the refined FE model with 2-node beam elements can accurately match the results of both experiments and conventional FE method. Moreover, the results of Figure 5 can be used as an optimization of patch lengths to reach the maximum possible deflection.

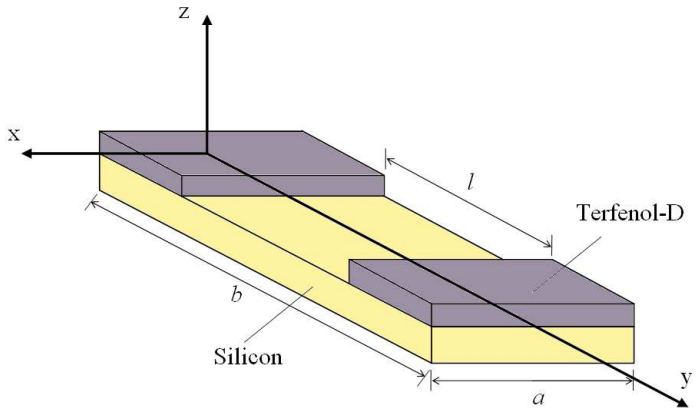

Figure 5: Silicon microbeam with magnetostrictive patches

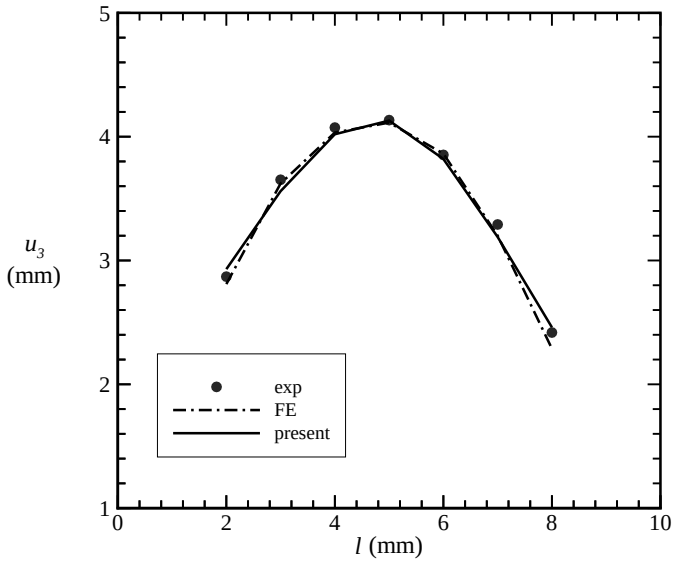

Figure 6: Microbeam maximum deflection (at $y = b/2$) for different uncoated lengths l of the beam

In order to get the accurate stress and strain distribution in the structure, the order and number of beam and cross-sectional elements should be increased. In other words, higher-order elements are needed to obtain continuous values for displacement derivatives. Therefore, 2, 3 and 4-node beam elements (B2, B3 and B4) are used for beam discretization while 4 and 9-node Lagrange elements (L4 and L9) are used as the expansion functions to model the cross-section, as shown in Figure 7.

The distribution of the normal stress component σ_{yy} across the beam thickness is plotted in Figure 8 for different beam element configurations, with 8L9 elements (see Figure 8-b). As it can be seen, five B3 elements in conjunction with eight L9 cross-sectional

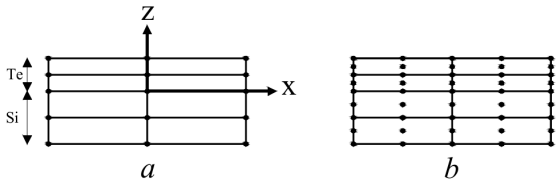

Figure 7: Cross-sectional Lagrange element configurations, a)8L4, b)8L9

elements can accurately predict the normal stress distribution through the thickness of the beam.

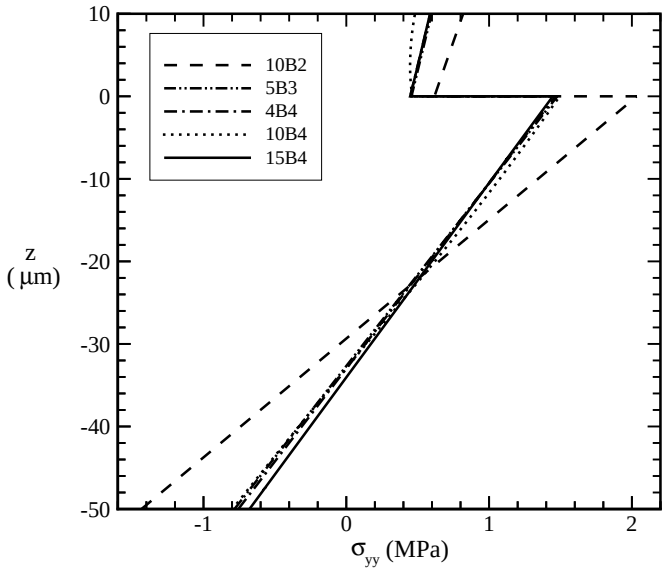

Figure 8: Distribution of normal stress σ_{yy} through the beam thickness at $x = 0$ and $y = 1$mm, for $l = 5$mm and $H_2 = 100$Oe

Figure 9 shows the distribution of the transverse shear stress component σ_{yz} across the beam thickness (8L9 elements). It can be clearly observed that B2 elements are not suitable for predicting the transverse shear stress. This is because the transverse shear stress component is related to the derivative of deflection with respect to the beam longitudinal axis coordinate, y. Since the variation of deflection is linear within each B2 element, the values of shear need to be corrected by a shear correction factor. However, when using higher-order elements, this problem is automatically fixed. In the absence of transverse mechanical loading, the overall shear stress through the thickness direction should vanish, as shown in Figure 9. However, at the interface of the substrate and the magnetostrictive patch, some shear stress is expected to be observed due to the horizontal shear forces induced by the elongation of magnetostrictive patch.

The variation of normal stress component σ_{yy} in the beam direction can also be achieved using B4 elements, as shown in Figure 10(8L9 elements). It can be seen that in the bimaterial parts of the beam, the normal stress in the silicon substrate is almost three times as in the Terfenol-D patch, as expected due to the Young modulus ratio. Furthermore, the maximum normal stress in each material occurs in the clamped end of the beam.

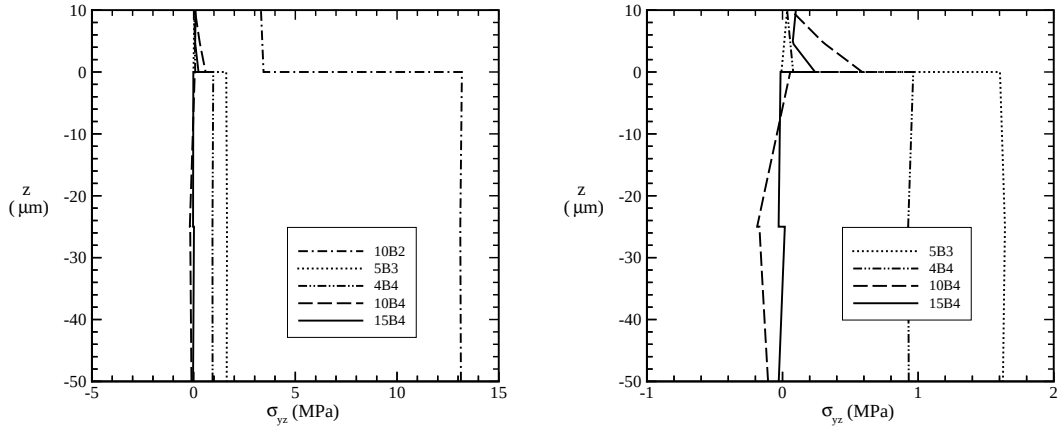

Figure 9: Distribution of shear stress σ_{yz} through the beam thickness at $x = 0$ and $y = 1$mm, for $l = 5$mm and $H_2 = 100$Oe, (Left)B2, B3 and B4 elements configuration,(Right) excluding B2 elements configuration

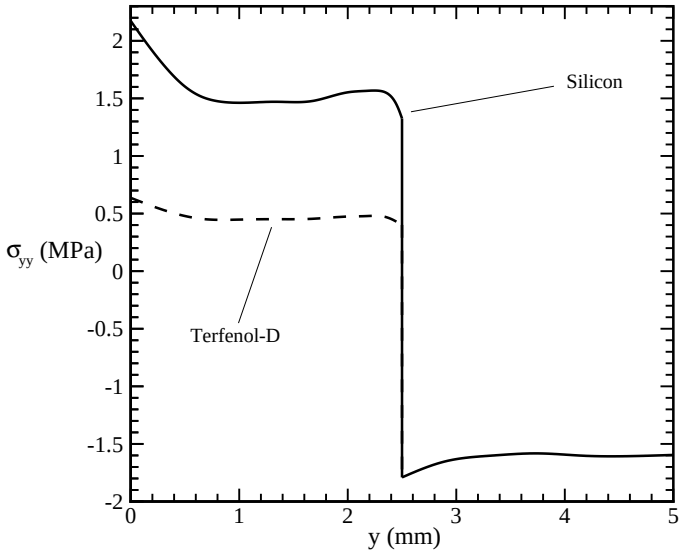

Figure 10: Distribution of stress σ_{yy} in the beam direction at $x = 0$ and $z = 0$mm, for $l = 5$mm and $H_2 = 100$Oe

4. Conclusions

In this paper, the well-known Carrera Unified Formulation is applied to the bending analysis of magnetostrictive unimorph microbeams as a one-dimensional refined Finite Element model. Through this formulations, using the principle of virtual displacement, the fundamental nuclei for the linear magnetomechanical coupled system are derived. The beam length is discretized using 2, 3 and 4-node beam elements, and the cross section is modeled using Lagrange expansions, with 4 and 8-node Lagrange elements. Finally, with application of mechanical and magnetic boundary conditions, the assembled linear algebraic system is solved to find the primary unknowns, namely, the displacement components and magnetic potential.

In order to illustrate the model, two examples of magnetostrictive micro-devices are stud-

ied and some numerical results have been presented. The results are first validated with the experimental and conventional finite element results, where the deflections have been shown to be in a good accordance. The normal and transverse shear stresses are then plotted as complementary results. It has been shown that the 2-node beam elements are enough to find the displacements, whereas at least 3-node beam elements should be adopted for estimating stresses. This work can be followed by application of the CUF to various other fields dealing with magnetostrictive multilayers, such as dynamic responses, modal analysis, buckling problems, etc. either with linear or nonlinear constitutive relations.

References

[1] J Aboudi, X Zheng, and K Jin. Micromechanics of magnetostrictive composites. *International Journal of Engineering Science*, 81:82–99, 2014.

[2] Y Hayashi, T Honda, KI Arai, K Ishiyama, and M Yamaguchi. Dependence of magnetostriction of sputtered tb-fe films on preparation conditions. *IEEE transactions on magnetics*, 29(6):3129–3131, 1993.

[3] T Honda, Y Hayashi, KI Arai, K Ishiyama, and M Yamaguchi. Magnetostriction of sputtered sm-fe thin films. *IEEE transactions on magnetics*, 29(6):3126–3128, 1993.

[4] T Honda, KI Arai, and M Yamaguchi. Fabrication of magnetostrictive actuators using rare-earth (tb, sm)-fe thin films. *Journal of Applied Physics*, 76(10):6994–6999, 1994.

[5] E Quandt, B Gerlach, and K Seemann. Preparation and applications of magnetostrictive thin films. *Journal of Applied Physics*, 76(10):7000–7002, 1994.

[6] E Quandt, A Ludwig, and K Seemann. Giant magnetostrictive multilayers for thin film actuators. In *Solid State Sensors and Actuators, 1997. TRANSDUCERS'97 Chicago., 1997 International Conference on*, volume 2, pages 1089–1092. IEEE, 1997.

[7] E Quandt, K Seemann, H Reichl, and A Heuberger. Micro systems technologies 96. *Berlin: VDE-Verlag*, 451, 1996.

[8] F Claeyssen, N Lhermet, J Betz, K Mackay, D Givord, E Quandt, and H Kronmuller. Linear and rotating magnetostrictive micro-motors. *Actuator 98*, pages 372–375, 1998.

[9] A Garnier, T Bourouina, H Fujita, T Hiramoto, E Orsier, and JC Peuzin. Magnetic actuation of bending and torsional vibrations for 2d optical-scanner application. *Sensors and Actuators A: Physical*, 84(1):156–160, 2000.

[10] T Bourouina, A Garnier, and H Fujita. Magnetostrictive microactuators and application to two-dimensional optical scanners. *Japanese journal of applied physics*, 41(3R):1608, 2002.

[11] E Klokholm. The measurement of magnetostriction in ferromagnetic thin films. *IEEE Transactions on Magnetics*, 12(6):819–821, 1976.

[12] E de Lacheisserie and JC Peuzin. Magnetostriction and internal stresses in thin films: the cantilever method revisited. *Journal of Magnetism and Magnetic Materials*, 136(1-2):189–196, 1994.

[13] PM Marcus. Magnetostrictive bending of a cantilevered film-substrate system. *Journal of magnetism and magnetic materials*, 168(1):18–24, 1997.

[14] M Weber, R Koch, and KH Rieder. Uhv cantilever beam technique for quantitative measurements of magnetization, magnetostriction, and intrinsic stress of ultrathin magnetic films. *Physical review letters*, 73(8):1166, 1994.

[15] E Van de Riet. Deflection of a substrate induced by an anisotropic thin-film stress. *Journal of applied physics*, 76(1):584–586, 1994.

[16] V Iannotti and L Lanotte. Improved model for the magnetostrictive deflection of a clamped film–substrate system. *Journal of magnetism and magnetic materials*, 202(1):191–196, 1999.

[17] WX Zhang, B Peng, HC Jiang, and SQ Yang. Influence of film thickness on deformation of a free magnetostrictive film-substrate system. *Journal of magnetism and magnetic materials*, 247(1):111–116, 2002.

[18] R Watts, MRJ Gibbs, WJ Karl, and H Szymczak. Finite-element modelling of magnetostrictive bending of a coated cantilever. *Applied physics letters*, 70(19):2607–2609, 1997.

[19] MEM Benbouzid, C Body, G Reyne, and C Meunier. Finite element modelling of giant magnetostriction in thin films. *IEEE Transactions on Magnetics*, 31(6):3563–3565, 1995.

[20] C Body, G Reyne, and G Meunier. Nonlinear finite element modelling of magneto-mechanical phenomenon in giant magnetostrictive thin films. *IEEE Transactions on Magnetics*, 33(2):1620–1623, 1997.

[21] HM Si and C Cho. Finite element modeling of magnetostriction for multilayered mems devices. *Journal of magnetism and magnetic materials*, 270(1):167–173, 2004.

[22] E Carrera, M Cinefra, M Petrolo, and E Zappino. *Finite element analysis of structures through unified formulation*. John Wiley & Sons, 2014.

[23] E Carrera and M Petrolo. On the effectiveness of higher-order terms in refined beam theories. *Journal of Applied Mechanics*, 78(2):021013, 2011.

[24] E Carrera, F Miglioretti, and M Petrolo. Computations and evaluations of higher-order theories for free vibration analysis of beams. *Journal of Sound and Vibration*, 331(19):4269–4284, 2012.

[25] E Carrera, G Giunta, P Nali, and M Petrolo. Refined beam elements with arbitrary cross-section geometries. *Computers & structures*, 88(5):283–293, 2010.

[26] E Carrera and A Pagani. Analysis of reinforced and thin-walled structures by multiline refined 1d/beam models. *International Journal of Mechanical Sciences*, 75:278–287, 2013.

[27] E Carrera, E Zappino, and M Petrolo. Analysis of thin-walled structures with longitudinal and transversal stiffeners. *Journal of Applied Mechanics*, 80(1):011006, 2013.

[28] SM Ibrahim, E Carrera, M Petrolo, and E Zappino. Buckling of composite thin walled beams by refined theory. *Composite Structures*, 94(2):563–570, 2012.

[29] A Pagani, M Boscolo, JR Banerjee, and E Carrera. Exact dynamic stiffness elements based on one-dimensional higher-order theories for free vibration analysis of solid and thin-walled structures. *Journal of Sound and Vibration*, 332(23):6104–6127, 2013.

[30] E Carrera and A Varello. Dynamic response of thin-walled structures by variable kinematic one-dimensional models. *Journal of Sound and Vibration*, 331(24):5268–5282, 2012.

[31] E Carrera and M Petrolo. Refined one-dimensional formulations for laminated structure analysis. *AIAA journal*, 50(1):176–189, 2012.

[32] A Pagani, E Carrera, M Boscolo, and JR Banerjee. Refined dynamic stiffness elements applied to free vibration analysis of generally laminated composite beams with arbitrary boundary conditions. *Composite Structures*, 110:305–316, 2014.

[33] E Carrera, A Pagani, and M Petrolo. Refined 1d finite elements for the analysis of secondary, primary, and complete civil engineering structures. *Journal of Structural Engineering*, 141(4):04014123, 2014.

[34] G Giunta, S Belouettar, and E Carrera. A thermal stress analysis of three-dimensional beams by refined one-dimensional models and strong form solutions. In *Applied Mechanics and Materials*, volume 828, pages 139–171. Trans Tech Publ, 2016.

[35] IA Ramos, JL Mantari, A Pagani, and E Carrera. Refined theories based on non-polynomial kinematics for the thermoelastic analysis of functionally graded plates. *Journal of Thermal Stresses*, 39(7):835–853, 2016.

[36] G Giunta, N Metla, S Belouettar, AJM Ferreira, and E Carrera. A thermo-mechanical analysis of isotropic and composite beams via collocation with radial basis functions. *Journal of Thermal Stresses*, 36(11):1169–1199, 2013.

[37] F Miglioretti, E Carrera, and M Petrolo. Variable kinematic beam elements for electro-mechanical analysis. *Smart Structures and Systems*, 13(4):517–546, 2014.

[38] F Biscani, Y Koutsawa, S Belouettar, and E Carrera. Effective properties of electro-elastic composites with multi-coating inhomogeneities. In *Advanced Materials Research*, volume 93, pages 190–193. Trans Tech Publ, 2010.

[39] Y Koutsawa, F Biscani, S Belouettar, H Nasser, and E Carrera. Multi-coating inhomogeneities approach for the effective thermo-electro-elastic properties of piezoelectric composite materials. *Composite structures*, 92(4):964–972, 2010.

[40] E Zappino, E Carrera, S Rowe, C Mangeot, and H Marques. Numerical analyses of piezoceramic actuators for high temperature applications. *Composite Structures*, 2016.

[41] E Carrera and M Petrolo. Refined beam elements with only displacement variables and plate/shell capabilities. *Meccanica*, 47(3):537–556, 2012.

[42] Y Shindo, F Narita, K Mori, and T Nakamura. Nonlinear bending response of giant magnetostrictive laminated actuators in magnetic fields. *Journal of Mechanics of Materials and Structures*, 4(5):941–949, 2009.